Astronomy & Astrophysics

Chemical abundances of distant extremely metal-poor unevolved stars[⋆,⋆⋆]

P. Bonifacio[1], L. Sbordone[2,1,3], E. Caffau[2,1,⋆⋆⋆], H.-G. Ludwig[2,1], M. Spite[1],
J. I. González Hernández[4,5], and N. T. Behara[6]

[1] GEPI, Observatoire de Paris, CNRS, Univ. Paris Diderot, Place Jules Janssen, 92190 Meudon, France
e-mail: Piercarlo.Bonifacio@obspm.fr
[2] Zentrum für Astronomie der Universität Heidelberg, Landessternwarte, Königstuhl 12, 69117 Heidelberg, Germany
[3] Max-Planck Institut für Astrophysik, Karl-Schwarzschild-Str. 1, 85741 Garching, Germany
[4] Instituto de Astrofísica de Canarias (IAC), 38205 La Laguna, Tenerife, Spain
[5] Depto. Astrofísica, Universidad de La Laguna (ULL), 38206 La Laguna, Tenerife, Spain
[6] Institut d'Astronomie et d'Astrophysique, Université Libre de Bruxelles, 1050 Bruxelles, Belgium

ABSTRACT

Context. The old Galactic halo stars hold the fossil record of the interstellar medium chemical composition at the time of their formation. Most of the stars studied so far are relatively near to the Sun, this prompts the study of more distant stars, both to increase the size of the sample and to search for possible variations of abundance patterns at greater distances.

Aims. The purpose of our study is to determine the chemical composition of a sample of 16 candidate extremely metal-poor (EMP) dwarf stars, extracted from the Sloan Digital Sky Survey (SDSS). There are two main purposes: in the first place to verify the reliability of the metallicity estimates derived from the SDSS spectra; in the second place to see if the abundance trends found for the brighter nearer stars studied previously also hold for this sample of fainter, more distant stars.

Methods. We used the UVES at the VLT to obtain high-resolution spectra of the programme stars. The abundances were determined by an automatic analysis with the `MyGIsFOS` code, with the exception of lithium, for which the abundances were determined from the measured equivalent widths of the Li I resonance doublet.

Results. All candidates are confirmed to be EMP stars, with [Fe/H] ≤ −3.0. The chemical composition of the sample of stars is similar to that of brighter and nearer samples. We measured the lithium abundance for 12 stars and provide stringent upper limits for three other stars, for a fourth star the upper limit is not significant, owing to the low signal-to noise ratio of the spectrum. The "meltdown" of the Spite plateau is confirmed, but some of the lowest metallicity stars of the sample lie on the plateau.

Conclusions. The concordance of the metallicities derived from high-resolution spectra and those estimated from the SDSS spectra suggests that the latter may be used to study the metallicity distribution of the halo. The abundance pattern suggests that the halo was well mixed for all probed metallicities and distances. The fact that at the lowest metallicities we find stars on the Spite plateau suggests that the meltdown depends on at least another parameter, besides metallicity.

Key words. stars: Population II – stars: abundances – Galaxy: abundances – Galaxy: formation – methods: data analysis – Galaxy: halo

1. Introduction

The Galactic halo contains some of the oldest stars in the Milky Way, and understanding its formation and evolution is one of the necessary steps to understand the Galaxy as a whole. Our ideas evolved in time, from the classical "monolithic collapse" scenario (Eggen et al. 1962), through the "chaotic" scenario (Searle & Zinn 1978) to the realisation that the halo has had a complex history and that both collapse and merging have contributed to its shaping (for a review see Helmi 2008, and references therein).

A milestone in the field was certainly the in situ study of the north Galactic pole by Majewski (1992) who showed that the halo appears to be counter-rotating. The panoramic view offered by modern wide-field surveys has allowed us to identify significant sub-structure in the halo, often referred to as the "field of

streams" (Belokurov et al. 2006). From the theoretical point of view, modern simulations predict that it is a general expectation that halos of spiral galaxies are built by a combination of in situ star formation and accretion from satellite dwarf galaxies (Zolotov et al. 2009; Font et al. 2011).

Exploiting the data of the Sloan Digital Sky Survey (SDSS and SEGUE York et al. 2000; Yanny et al. 2009), Carollo et al. (2007, 2010) showed that the Galactic stellar halo is composed of at least two components with distinct kinematics and metallicity distribution, the more distant halo being more metal-poor. This analysis was based on relatively bright stars in SDSS, for which accurate proper motions could be derived. The SDSS catalogue contains spectra and photometry down to $g = 20$, suggesting that an in situ study of the distant halo is indeed possible.

With this in mind we began in 2006 to work on the analysis of SDSS spectra with two main goals: 1) retrieve from SDSS candidate stars of extremely low metallicity for high-resolution follow-up; 2) determine the metal-weak tail of the halo metallicity distribution function directly from the SDSS spectra.

The first goal was motivated to see if there is indeed a metallicity threshold for the formation of low-metallicity stars, as suggested by some theories of star formation at low metallicity (Schneider et al. 2003; Bromm & Loeb 2003; Salvadori et al. 2007), and to check the hypothesis that at very low abundances of iron only stars with strong enhancements of C and O can be found (Bromm & Loeb 2003; Frebel et al. 2007).

The second goal is straightforward. The metallicity distribution function (MDF) provides a strong constraint on the theories of galaxy formation and evolution, especially at the low-metallicity end. The current versions of the MDF are based on a limited number of stars (Ryan & Norris 1991; Schörck et al. 2009; Li et al. 2010), a few thousands at most. The SDSS has the potentiality of doing this for a sample of stars that is two orders of magnitudes larger. For this to be possible, though, two steps are necessary: 1) the abundance estimated from the low-resolution SDSS spectra must be confidently calibrated against abundances derived from high-resolution spectra; 2) the selection biases in the SDSS sample must be understood.

It is clear that our goals require that extremely metal-poor (EMP) candidates extracted from the SDSS should be observed at higher resolution. To this end we carried out several observational campaigns at the European Southern Observatory with the UVES (Dekker et al. 2000) and X-Shooter (D'Odorico et al. 2006) spectrographs. Over the years we have made three progress reports (Ludwig et al. 2008; Bonifacio et al. 2010; Sbordone et al. 2010b) on this programme. The abundances of three C-enhanced dwarf stars, observed with UVES, have been reported in Behara et al. (2010), and the abundances for two stars observed with X-Shooter in Bonifacio et al. (2011). In this paper we report the abundances for 16 stars of typical magnitude $g \sim 17$, observed with UVES in the course of ESO periods 78 and 81. In an accompanying papers (Caffau et al. 2011b) we reported the abundances of five stars observed with X-Shooter. Finally, in Caffau et al. (2011c, 2012) we described the most metal-poor star found in the sample, observed with both X-Shooter and UVES.

2. Target selection

The programme stars were selected from the SDSS Data Releases 5 (Adelman-McCarthy et al. 2007) and 6 (Adelman-McCarthy et al. 2008). Names, coordinates, and g magnitudes are provided in Table 4. To obtain spectra of good quality in a limited amount of time with UVES, based on the exposure time calculator and on our personal experience with this instrument, we restricted the sample to $g \leq 17.5$. We decided to focus on turn-off (TO) stars, for several reasons. In the first place the surface gravity can be confidently fixed at $\log g = 4.0$ for these stars, a minor contaminant being Horizontal Branch stars of higher luminosity. According to the Padova isochrone of metallicity –2.0 and age of 13 Gyr (Marigo et al. 2008), the absolute g magnitude of TO stars ranges between 3.0 and 3.6. This implies, if one neglects interstellar extinction, a distance range between roughly 6 kpc and 8 kpc, these objects are thus capable to probe the outer halo. In this phase of the project we aimed to avoid the complication of discriminating between K dwarfs and K giants, although in the future we do intend to tackle cooler stars, because K giants allow one to probe considerably greater distances. Another reason is that the SDSS spectroscopic sample is very rich in TO-colour objects. There are two factors that contributed to boost their number: metal-poor F dwarfs were often observed as suitable flux-calibration standards, and the SDSS QSO selection

algorithm (Richards et al. 2002) also selects very metal-poor TO stars.

To select the TO stars we relied on the $(g - z)_0$ colour, which we calibrated against T_{eff} (Ludwig et al. 2008), our initial selection was $-0.3 \leq (g - z)_0 \leq 0.7$, which, in terms of T_{eff}, corresponds to: $5500 \leq T_{\mathrm{eff}} \leq 8000$ K. Our initial sample consisted of about 34 000 stars. The motivation for including these high effective temperatures was to be able to capture the EMP stars with C-enhanced composition predicted by the isochrones of Piau et al. (2006).

The raw metallicity distribution function is shown in Fig. 3 of Ludwig et al. (2008). The almost flat behaviour at metallicities below −4.0 is clearly suspicious. It should be emphasized that at these low metallicities the only metallic line measurable on SDSS spectra for TO stars is the Ca II K line. Visual inspection of all SDSS spectra of the sample, with estimated metallicity below −3.0 showed that in fact the low-metallicity sample was dominated by white dwarfs, some of which do show a measurable Ca II K line in the SDSS spectra. At this stage we also realised that the vast majority of the white dwarfs could indeed be excluded by a simple cut on the $(u - g)_0$ colour: $(u - g)_0 > 0.70$. The cleaned sample with a more restrictive temperature cut $0.18 \leq (g - z)_0 \leq 0.70$ consisted of about 26 000 stars. The metallicity distribution function was presented in Bonifacio et al. (2010) and shows no flattening at low metallicity. We have already used these cuts on data of SDSS Data Release 7 (see Caffau et al. 2011b) and we will use it on SDSS Data Release 8. These more restricted colour cuts will not be able to select the stars predicted by Piau et al. (2006), if they exist. We point out that finding these objects among the white dwarfs of similar colours is fairly challenging.

The final selection of the targets to be observed with UVES had to take into account the observability conditions from Paranal ($\delta \leq +28$) and was made by visual inspection of all stars with [Fe/H]$_{\mathrm{SDSS}} \leq -3.0$. It was not our purpose to observe a sample of stars with a well-defined selection function, but rather to observe a sample of true EMP stars. The three stars reported in Behara et al. (2010) were already recognized at this stage as C-enhanced stars.

For the reader's convenience an excerpt of the SDSS photometry for our programme stars is provided in Table 3. Full information is available on the SDSS site www.sdss.org.

3. UVES observations and data reduction

The observations were obtained in the course of two ESO periods, both programmes had Ludwig as PI. In period 78 we were allocated 29 h in service mode, in period 81 we were allocated three nights in visitor mode. A log of the observations, including the slit width and CCD binning is given in Table 1, more details on each observation are available through the ESO archive[1]. We only remark that in the visitor run of April 2008 (observer L. Sbordone) we lost almost half of the time, due to strong northern wind, which prohibited pointing of our targets. The run of August 2008 (observer Ludwig) was instead quite succesful. The instrumental set-up was similar for the service and the visitor-mode observations. In both cases we used the

---

[1] http://archive.eso.org/wdb/wdb/eso/eso_archive_main/query?prog_id=078.D-0217(A)
http://archive.eso.org/wdb/wdb/eso/eso_archive_main/query?prog_id=081.D-0373(A)
http://archive.eso.org/wdb/wdb/eso/eso_archive_main/query?prog_id=081.D-0373(B)
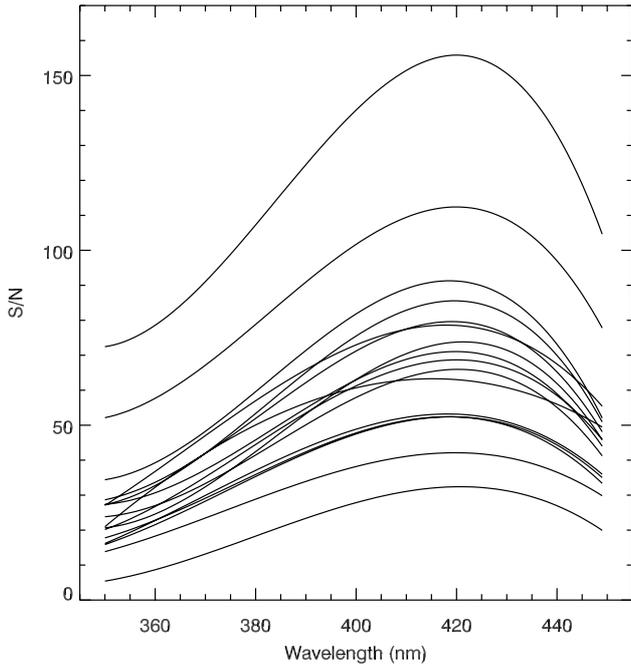
Fig. 1. The signal-to-noise ratio as a function of wavelength in the blue-arm spectra. This is a by-product of `MyGIsFOS`, which calculates it in all the continuum regions.

Fig. 2. Portion of the spectrum of SDSS J122935+262445, one of the lowest S/N spectra in our sample. The boxes show the wavelength intervals used to fit the lines (blue for Fe I lines, green the Si I line, red the Ti II line), when they are shaded it means that MyGIsFOS has rejected the line. Two boxes showing continuum regions are also shown (grey boxes). Horizontal dashed and dotted lines indicate the local 1σ and 3σ estimated noise ranges. Vertical magenta continuous and dashed lines (in the top part of the plot) indicate by how much every single line has been shifted in radial velocity by MyGIsFOS to achieve an optimal fit.

dichroic # 1 390+580 nm setting. In the service mode we used a 1″4 wide slit and 2 × 2 on-chip binning. This was made to collect as many photons as possible for these faint stars, however, if the seeing was less than the slit width, the actual resolution was set by the seeing. In the visitor observations, the same philosphy was employed, but if the observer noticed that the seeing was much smaller than the slit width he had the opportunity of narrowing the slit width and, if the chosen slit width was less than, or equal to 0″8, also to change the binning to 1 × 1 binning. The data of period 78 were retrieved reduced from the ESO archive, we reduced the observations of period 81 using the UVES pipeline.

For each star we had several spectra of slightly different resolution. To combine the spectra, we estimated the actual resolution from a number of unblended lines and then convolved each spectrum with a Gaussian so that the final resolution was either 13.9 km s^{-1} or 12 km s^{-1}.

Two stars, SDSS J002113–005005 and SDSS J004029+160416 were observed both in period 78 and period 81. We decided to analyse the two sets of spectra independently to obtain a consistency check.

The signal-to-noise ratios obtained are shown in Fig. 1 for the blue arm, where this ratio is lowest.

Star SDSS J153110+095255 was observed in ESO period 81, a preliminary analysis confirms that its metallicity is about −3.0, yet the star is double-lined spectroscopic binary. This star was excluded from the present sample and will be analysed when more spectra are available.

4. Abundance analysis

The analysis was performed with the `MyGIsFOS` code (Sbordone et al. 2010b; Sbordone et al., in prep.). The code evolved from the code of Bonifacio & Caffau (2003), and was entirely re-coded in `fortran 90` with several improvements. Briefly: this program compares the observed spectrum to a grid of synthetic
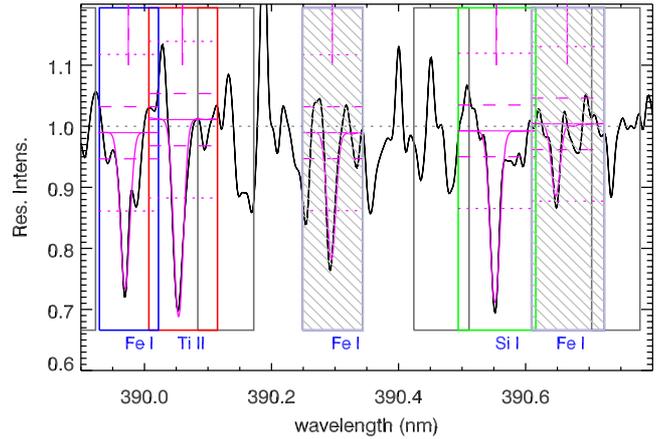
spectra and performs χ^2 fitting. The most noticeable improvement is a loop to determine the surface gravity from the iron ionisation equilibrium. The grid of synthetic spectra was computed from a grid of ATLAS 12 (Kurucz 2005; Castelli 2005; Sbordone et al. 2004; Sbordone 2005) model atmospheres. Convection was treated in the mixing-length approximation with $\alpha_{MLT} = 1.25$. The grid covers the effective temperatures 5400–7000 K at steps of 200 K, logarithmic surface gravities 3.5–4.5 (cgs units) at steps of 0.5 dex, logaritmic metallicities in the range −4.0 to −2.0, at steps of 0.5 dex, [α/Fe] = 0.0, +0.4 and microturbulent velocities of 1, 2, 3 km s^{-1}.

The effective temperature was considered a prior and was derived from the $(g − z)_0$ colour using the calibration presented in Ludwig et al. (2008). We checked the effective temperatures also with fits of the wings of Hα based on CO^{5}BOLD models, as in Sbordone et al. (2010a), these provide temperature that are hotter, on average, by 116 K. In five cases the fits required extrapolation beyond the range of the CIFIST grid (Ludwig et al. 2009). We decided to keep the photometric temperatures, to make the comparison of the metallicities with those derived from the SDSS spectra straightforward. The surface gravity was determined from the iron ionisation equilibrium. If no Fe II lines were retained in the analysis, then the surface gravity was held fixed at the starting value, log g = 4.0. The ratio [α/Fe] was determined from the Mg and Ca lines. The solar abundances adopted are given in Table 2, Fe is from Caffau et al. (2011a), the other elements are from Lodders et al. (2009).

Two examples of fits performed by `MyGIsFOS` are shown in Figs. 2 and 3, illustrating the capability of `MyGIsFOS` to reject poor fits. That we recovered the same abundances, within errors, for the two stars for which we analysed the spectra observed in period 78 and 81 independently, reassures us about the robustness and reproducibility of `MyGIsFOS`.

The resulting chemical abundances are provided in Tables 5 and 6. For chemical species for which several lines are measurable, we provide the standard deviation of the abundances derived from the different lines (line-to-line scatter). This can be assumed to be a reasonable estimate of the error on the provided
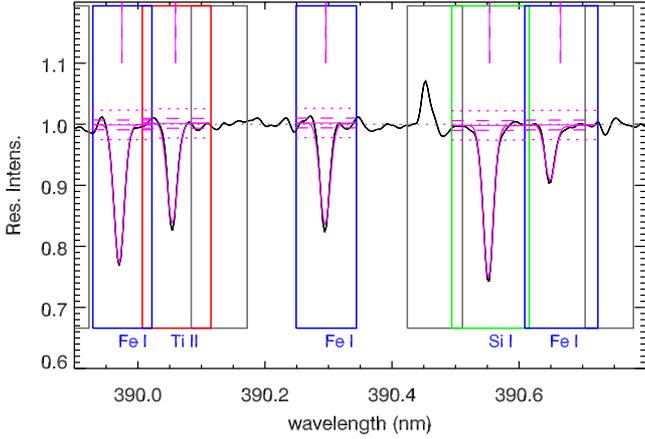
Fig. 3. Same as Fig. 2, but for SDSS J004029+160416 observed in period 81, probably the best spectrum of the sample. In this case none of the lines is rejected.

Table 2. Adopted solar abundances.

Element	log(X/H) +12
Mg	7.54
Si	7.52
Ca	6.33
Sc	3.10
Ti	4.90
Cr	5.64
Mn	5.37
Fe	7.52
Co	4.92
Ni	6.23
Sr	2.92

Table 3. Sloan photometry for the programme stars.

Star	r	$(g - z)$	$(g - z)_0$	$(u - g)$	$(u - g)_0$
SDSS J002113–005005	16.468	0.28	0.21	0.94	0.90
SDSS J002749+140418	16.537	0.62	0.39	1.06	0.93
SDSS J004029+160416	15.279	0.36	0.26	0.94	0.88
SDSS J031745+002304	16.367	0.74	0.54	0.95	0.83
SDSS J082118+181931	16.817	0.36	0.30	0.85	0.81
SDSS J082521+040334	16.441	0.45	0.35	0.94	0.89
SDSS J090733+024608	16.010	0.50	0.44	0.95	0.91
SDSS J113528+010848	16.434	0.44	0.38	0.90	0.87
SDSS J122935+262445	16.420	0.31	0.25	0.88	0.84
SDSS J130017+263238	15.970	0.30	0.28	0.85	0.84
SDSS J143632+091831	15.806	0.37	0.30	0.83	0.79
SDSS J144640+124917	15.902	0.41	0.36	0.86	0.83
SDSS J154246+054426	16.853	0.52	0.36	0.87	0.78
SDSS J223143–094834	16.519	0.54	0.42	0.86	0.79
SDSS J230814–085526	16.147	0.53	0.44	0.82	0.77
SDSS J233113–010933	17.192	0.42	0.34	0.90	0.85

abundance or abundance ratio. The different quality (S/N ratio) of the spectra is immediately reflected in the line-to-line scatter of a species with many lines available, such as Fe I. This is indeed illustrated in Fig. 4. For species for which only one line is available the error could be estimated from the S/N in the spectrum at the wavelength of the line. With the spectra at hand this should be in the range 0.1–0.2 dex.

The systematic error caused by the uncertainty in atmospheric parameters has been treated in many papers. For an estimate we refer the readers to Table 4 of Bonifacio et al. (2009), the systematic errors in our analysis are essentially the same.
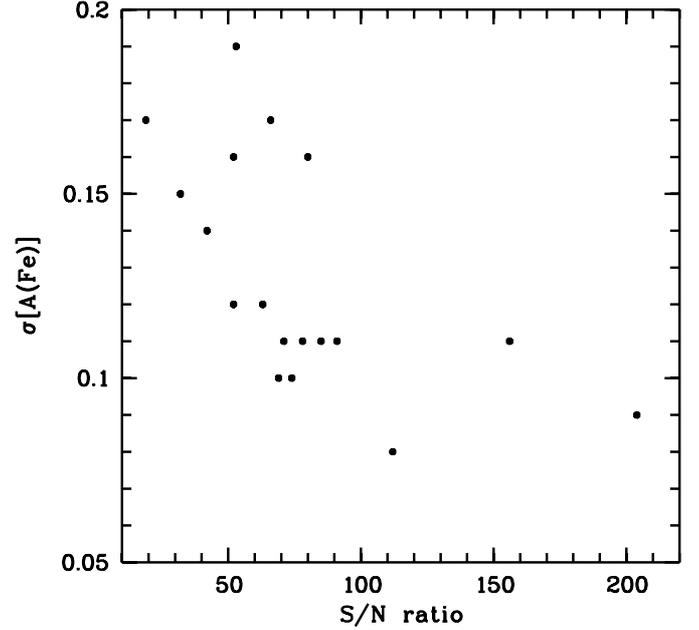
Fig. 4. Line-to-line scatter in the Fe I abundances as a function of the S/N ratio at 420 nm. There is a clear correlation between the two.

For lithium we did not use MyGIsFOS, but we measured the equivalent widths by fitting synthetic profiles, as described in Bonifacio et al. (2002) and then determined the lithium abundances by using the fitting formula of Sbordone et al. (2010a), based on CO⁵BOLD 3D models (Freytag et al. 2002; Wedemeyer et al. 2004; Freytag et al. 2012) and NLTE treatment of line transfer. For the stars for which we could not detect the Li doublet we estimated the upper limit at 3σ by using the Cayrel formula (Cayrel 1988). The results are provided in Table 7.

Star SDSS J090733+024608 is in common between us and Caffau et al. (2011b), the abundances derived by us from the UVES spectrum of this star agree excellently with those derived by Caffau et al. (2011b) from the X-Shooter spectrum.

5. Distances

Using the SDSS photometry and theoretical isochrones, it is possible to estimate the distances of our sample of stars. We used the Padova isochrone (Girardi et al. 2002) with $Z = 0.0001$ and an age of 13.5 Gyr. To read the absolute magnitude from the isochrone it is necessary to decide whether a star is above or below the turn-off. For any set of atmospheric parameters we assumed the star is on the Main Sequence (MS, i.e. it is *below* the TO) if $\log g \geq 4.18$ and on the sub giant branch (SG, i.e. is *above* the TO) if $\log g < 4.18$. This distinction is based on the estimated surface gravity of the TO from the theoretical isochrone. In Table 8 we provide the distances, d, from the Sun derived in this way, averaged over the five SDSS bands, in kpc. In the column σ_d we provide the standard deviation of the distances derived from the different bands. This should not be used as an estimate for the errors on our distances, but only as a sanity check of the consistency of the photometry in the different bands. For star SDSS J090733+024608 Caffau et al. (2011b) estimate a distance that is about 1 kpc larger, becasue they chose a different isochrone. This difference can be taken as an estimate of the uncertainty on our distances.

We also provide the distances from the Galactic centre, computed as $R = \sqrt{d^2 - 2dR_{GC} \cos(b) \cos(l) + R_{GC}^2}$ where R_{GC} is

Table 4. Coordinates and atmospheric parameters for the programme stars.

Star	g mag	α J2000	δ J2000	$T_{\rm eff}$ K	$\log g$ cgs	ξ km s^{-1}	[Fe/H]	S/N @420 nm	ESO period SDSS Object Type[a]	
SDSS J002113–005005	16.7	00:21:13.78	–00:50:05.2	6546	4.59	1.54	−3.15	52	78	QSO
				6546	4.01	1.76	−3.25	74	81	QSO
SDSS J002749+140418	16.9	00:27:49.46	+14:04:18.1	6125	3.61	1.46	−3.37	69	78	SP STD
SDSS J004029+160416	15.5	00:40:29.17	+16:04:16.2	6422	3.88	1.48	−3.27	112	78	Ser BLUE
				6422	3.93	1.58	−3.25	156	81	Ser BLUE
SDSS J031745+002304	16.8	03:17:45.82	+00:23:04.2	5786	4.02	1.41	−3.46	66	78	SP STD
SDSS J082118+181931	16.7	08:21:18.18	+18:19:31.8	6158	4.00	1.50	−3.80	19	78	SP STD
SDSS J082521+040334	17.1	08:25:21.29	+04:03:34.4	6340	4.00	1.23	−3.46	80	81	SP STD
SDSS J090733+024608	16.3	09:07:33.28	+02:46:08.2	5934	3.71	1.61	−3.44	204	78	SP STD
SDSS J113528+010848	16.7	11:35:28.08	+01:08:48.8	6132	3.83	1.65	−3.03	63	78	SP STD
SDSS J122935+262445	16.7	12:29:35.95	+26 24 45.9	6452	4.20	2.68	−3.29	32	81	SP STD
SDSS J130017+263238	16.2	13:00:17.20	+26:32:38.6	6393	4.00	1.36	−3.65	85	81	SP STD
SDSS J143632+091831	16.1	14:36:32.27	+09:18:31.5	6340	4.00	1.42	−3.40	53	78	SP STD
SDSS J144640+124917	16.1	14:46:40.63	+12:49:17.6	6189	3.90	1.77	−3.16	52	78	SP STD
SDSS J154246+054426	17.2	15:42:46.87	+05:44:26.4	6179	4.00	1.68	−3.48	78	78	SP STD
SDSS J223143–094834	16.9	22:31:43.95	–09:48:34.4	6053	4.16	1.36	−3.20	91	78	SP STD
SDSS J230814–085526	16.5	23:08:14.85	–08:55:26.4	6015	4.66	1.74	−3.01	42	78	SP STD
SDSS J233113–010933	17.5	23:31:13.50	–01:09:33.4	6246	4.21	1.38	−3.08	71	81	RED STD

Notes. [a] Object type, based on colours that motivated the selection of this object for SDSS spectroscopy: QSO = quasi stellar object; SP STD = spectrophotometric standard; Ser BLUE = serendipity blue object; RED STD = reddening standard.

Table 5. Abundances of the α elements and strontium.

Star	[Fe/H]	[Mg/Fe]	σ	N	[Si/Fe]	N	[Ca I/Fe]	σ	N	[Ca II/Fe]	N	[Ti I/Fe]	σ	N	[Ti II/Fe]	σ	N	[Sr/Fe]	σ	N
SDSS J002113–005005	−3.15	+0.13	0.16	3	+0.02	1				+0.53	1				+0.75		6	−0.31		2
	−3.25	+0.18	0.14	2			+0.72		1	+0.46	1				+0.66	0.14	8	−0.45		1
SDSS J002749+140418	−3.37	+0.17	0.11	3	−0.11	1	+0.40	0.22	2	+0.36	1				+0.22		6	−0.69		2
SDSS J004029+160416	−3.27	+0.33	0.14	3	+0.10	1	+0.28	0.08	2	+0.41	1				+0.57	0.15	12	−0.53		1
	−3.25	+0.25	0.17	2	+0.10	1	+0.38	0.11	2	+0.50	1	+1.09		1	+0.52	0.13	12	−0.56		1
SDSS J031745+002304	−3.46	+0.38	0.21	4			+0.60		1	+0.75	1	+1.04		1	+0.43	0.25	3	−0.85		1
SDSS J082118+181931	−3.80	+0.24	0.17	2																
SDSS J082521+040334	−3.46	+0.35	0.19	3	+0.20	1				−0.16	1				−0.06		1			
SDSS J090733+024608	−3.44	+0.30	0.09	2			+0.51		1	+0.31	1	+0.82		1	+0.58	0.15	11	−0.23		1
SDSS J113528+010848	−3.03	+0.15	0.14	3			+0.45	0.13	2						+0.49	0.20	9	+0.50	0.16	2
SDSS J122935+262445	−3.29	+0.22	0.20	4	+0.08	1				+0.79	1				+0.78	0.36	4	+0.23	0.10	2
SDSS J130017+263238	−3.65	+0.53	0.13	2	+0.75	1				+0.48	1				+0.31	0.11	2			
SDSS J143632+091831	−3.40	+0.39	0.21	2	+0.09	1	+0.87		1	+0.44	1				+0.77	0.25	2	−0.41		1
SDSS J144640+124917	−3.16	−0.04		1	−0.03	1	+0.51		1	−0.26	1				+0.14	0.18	5			
SDSS J154246+054426	−3.48	+0.20	0.11	3	+0.31	1				−0.07	1				−0.00	0.14	2			
SDSS J223143–094834	−3.20	+0.30	0.12	2	+0.38	1	+0.47	0.16	6	+0.15	1	+0.77	0.18	2	+0.43	0.15	6	+0.07	0.07	2
SDSS J230814–085526	−3.01	+0.03	0.20	3			+0.28	0.14	2	−0.06	1				+0.42		7	−0.78		1
SDSS J233113–010933	−3.08	−0.05	0.11	2	−0.05	1				+0.08	1	+0.93		1	+0.23	0.26	5			

the Sun-Galactic centre distance, taken to be 8.5 Kpc, l, b are Galactic longitude and latitude. As expected from their faintness, the stars are distant.

In the last column of Table 8 we also provide the barycentric radial velocities, computed by cross-correlation of the blue spectra against a synthetic template, after masking out the Balmer lines. For the stars for which we have multiple observations the standard deviation of the different radial velocities never exceeds 0.6 km s^{-1}, thus none of the stars shows any radial velocity variations. The radial velocity accuracy is dominated by the systematics, and mainly by the centering of the star in the slit. The plate scale of the UVES blue arm (0.″215 or 0.0019 nm in the dispersion direction) implies that an error of 0.″2 in centering, corresponds to 1.3 km s^{-1}, this can be taken as an estimate of the absolute error on radial velocities. Our measured radial velocity for SDSS J090733+024608 agrees excellently with the measurement of Caffau et al. (2011b) from their X-Shooter spectrum.

Bonifacio et al. (2009) did not estimate distances for their sample of stars, and it is beyond the purpose of the present paper to provide such estimates for those stars. Suffice it to say that the V magnitudes of the Bonifacio et al. (2009) sample range from 13 to 15.2, while most of the stars in the present sample have g magnitudes between 16 and 17.5. Given that V and g magnitudes are fairly similar for stars of these spectral types, we expect the stars of the present sample to be on average four times more distant[2].

6. Discussion

The first thing to remark is the quite good performance of the [Fe/H] estimates obtained from the SDSS spectra, down to

---

[2] If two stars have the same absolute magnitude and different apparent magnitudes m_1 and m_2, the ratios of their distances is $\log(d_1/d_2) = (m_1 - m_2)/5$. Thus if $m_1 - m_2 = 3$, then $d_1 \approx 4d_2$.

Table 6. Abundances of the iron peak elements.

Star	[Fe I/H]	σ	N	[Fe II/H]	σ	N	[Sc/Fe]	N	[Cr/Fe]	σ	N	[Mn/Fe]	σ	N	[Co/Fe]	σ	N	[Ni/Fe]	σ	N
SDSS J002113–005005	−3.15	0.16	36	−3.15		1												+0.05	0.34	5
	−3.25	0.10	38	−3.26	0.12	3			+0.13	0.24	2							+0.10	0.25	4
SDSS J002749+140418	−3.37	0.10	40	−3.37		1			−0.18	0.22	4	−0.24	0.22	2				+0.06	0.14	5
SDSS J004029+160416	−3.27	0.08	43	−3.27	0.09	3			−0.12	0.11	4							−0.05	0.15	6
	−3.25	0.11	43	−3.25	0.05	2	+0.19	1	−0.22	0.23	3	−0.67		1	+0.49		1	−0.04	0.13	8
SDSS J031745+002304	−3.46	0.17	42	−3.46	0.13	3	+0.17	1	−0.47	0.18	2	−0.52		1	+0.58		1	+0.01	0.23	8
SDSS J082118+181931	−3.80	0.17	5																	
SDSS J082521+040334	−3.46	0.16	36				+0.30	1				−0.01		1				+0.48	0.21	4
SDSS J090733+024608	−3.44	0.09	47	−3.44		1	+0.22	3	−0.32	0.17	5				+0.70	0.21	3	+0.07	0.14	7
SDSS J113528+010848	−3.03	0.12	54	−3.03	0.11	2	+0.12	1	−0.08	0.13	3	−0.14	0.08	2	+0.50		1	+0.32	0.17	9
SDSS J122935+262445	−3.29	0.15	29	−3.29	0.03	2			+0.16		1									
SDSS J130017+263238	−3.65	0.11	30																	
SDSS J143632+091831	−3.40	0.19	34															+0.00	0.24	2
SDSS J144640+124917	−3.16	0.12	40	−3.15	0.06	2	+0.29	1	+0.06	0.17	3	−0.08	0.11	3				+0.07	0.25	6
SDSS J154246+054426	−3.48	0.11	34						−0.19		1							+0.31	0.16	6
SDSS J223143–094834	−3.20	0.11	47	−3.20	0.03	3	+0.11	1	−0.22	0.13	4	−0.47	0.05	2	+0.44	0.12	3	−0.02	0.22	10
SDSS J230814–085526	−3.01	0.14	50	−3.01		1	+0.49	1	−0.32	0.17	3	−0.25	0.16	2	+0.64		1	+0.29	0.16	7
SDSS J233113–010933	−3.08	0.11	42	−3.08	0.24	2			−0.28	0.18	4	−0.32	0.05	3	+0.56		1	+0.21	0.22	6

Table 7. Abundances of lithium in the programme stars.

Star	EW (pm)	A(Li)
SDSS J002113–005005	1.26	2.08
	1.69	2.21
SDSS J002749+140418	2.60	2.13
SDSS J004029+160416	1.31	2.02
	1.32	2.03
SDSS J031745+002304	3.05	1.97
SDSS J082118+181931	<0.98	<1.71
SDSS J082521+040334	1.43	2.02
SDSS J090733+024608	4.15	2.23
SDSS J113528+010848	1.87	1.99
SDSS J122935+262445	0.92	1.88
SDSS J130017+263238	1.66	2.10
SDSS J143632+091831	<0.45	<1.48
SDSS J144640+124917	0.77	1.62
SDSS J154246+054426	1.68	1.97
SDSS J223143–094834	<0.37	<1.20
SDSS J230814–085526	<0.60	<1.39
SDSS J233113–010933	2.64	2.22

Fig. 5. Difference between the [Fe/H] derived from the UVES spectra and that derived from the SDSS spectra as a function of [Fe/H]$_{SDSS}$. Evidently down to [Fe/H] ∼ −3.5 is accurate to about 0.2 dex, but rapidly increases below. The open symbols are the stars observed with X-Shooter by Caffau et al. (2011b). The star symbol is SDSS J102915+172927 (Caffau et al. 2011c).

about [Fe/H] = −3.5. Owing to the few objects at lowest metallicity no definite conclusion can be drawn whether the metallicity estimates based on SDSS spectra are biased. However, the low metallicity of SDSS J102915+172927 (Caffau et al. 2011c) indicates that this is not very likely.

The fact that at low metallicity the estimate based on SDSS spectra relies essentially on the Ca II K line implies that the method is prone to underestimate the abundances of stars that are not enhanced in α elements, as discussed in Bonifacio et al. (2011).

Considering the results of the present paper, of Caffau et al. (2011b) and Caffau et al. (2011c, 2012) together allows us to conclude that the metallicities estimated from the SDSS spectra are reliable, in a statistical sense, at least down to [Fe/H] = −5. The study of the halo metallicity distribution based on the SDSS spectra will be adressed in a future paper.

The results on the chemical composition of the present sample of stars suggests that, by and large, they are "typical" halo stars compared to the sample of Bonifacio et al. (2009), as we did in Figs. 6 to 9. Below we remark on the groups of elements.
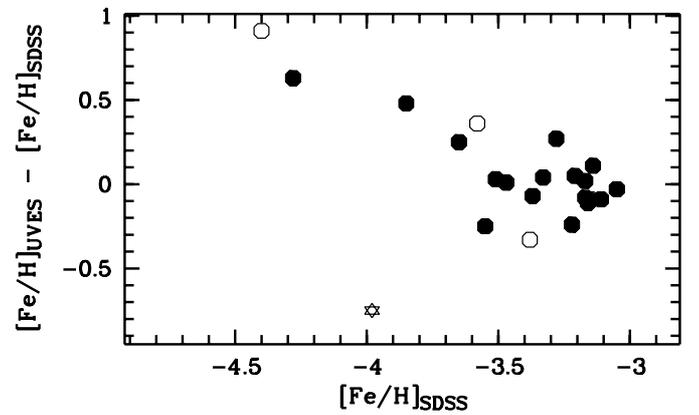
6.1. α elements

In Fig. 6 we compare the present results with those of Bonifacio et al. (2009), which were rescaled to the solar abundances here adopted. The abundance ratios of our stars show a larger scatter than those of Bonifacio et al. (2009) and we interpret this result as caused by the lower S/N ratio of our spectra. The [Ca/Fe] ratio in the figure is the straight average of the abundance derived from Ca I lines and the Ca II 370.6024 nm, when both are available, although in several cases there is a sizeable difference in the two abundances, this could arise from an incorrect gravity. The most striking case is that of SDSS J144640+124917, for which the Ca I 445.4779 nm line provides [Ca/Fe] = +0.51, while the Ca II 370.6024 nm, provides [Ca/Fe] = −0.26. The current version of MyGIsFOS adjusts the gravity only on the iron ionisation equilibrium, use of other elements is possible in future implementations. Two stars, SDSS J082521+040334 and SDSS J154246+054426 show a negative [Ca/Fe], based only on the Ca II 370.6024 nm line, remarkably, they also show a negative [Ti/Fe], although both have standard enhancement of Si and Mg.
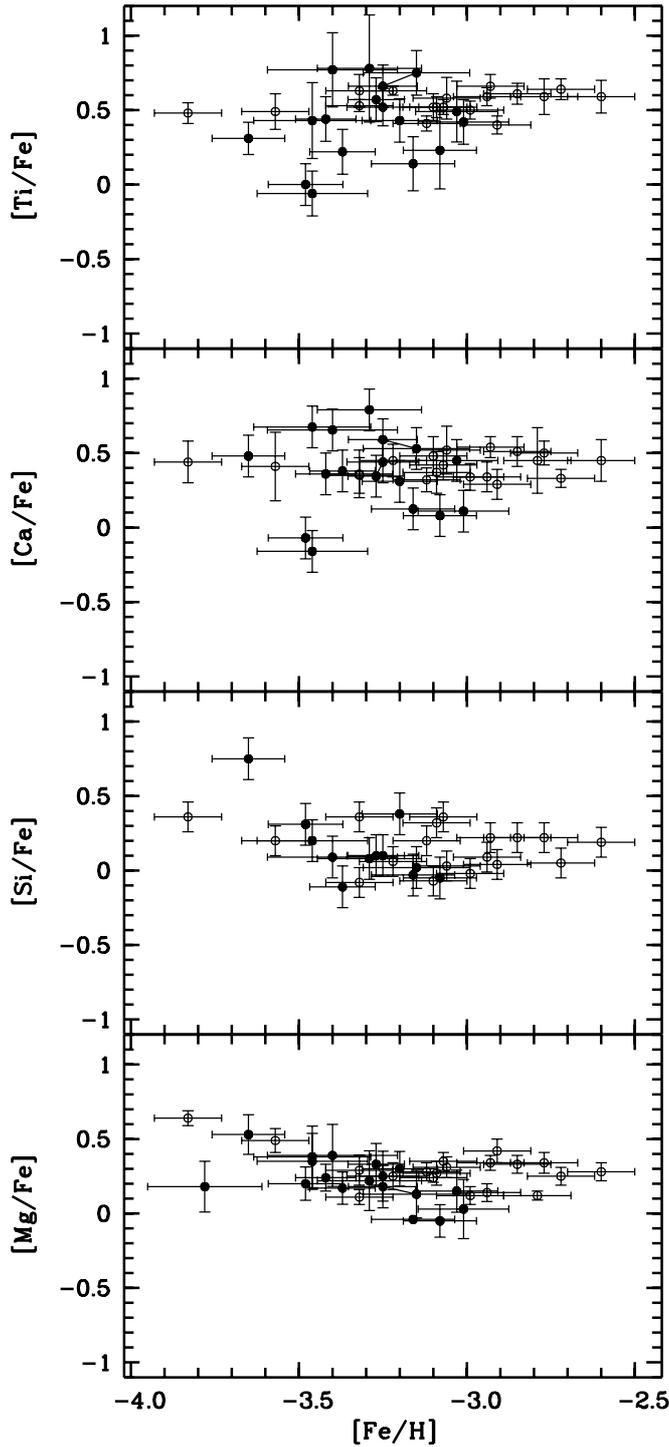
Fig. 6. Ratios of alpha elemements to iron for our programme stars (filled circles) compared to those of the stars of Bonifacio et al. (2009) (open circles). The spectra of SDSS J004029+160416 and SDSS J002113-005005 observed in periods 78 and 81 were treated independently and the points referring to the derived abundances are connected by a line. The one referring to the two measures of SDSS J004029+160416 is not visible, since the two points are indistinguishable at the resolution of the plot.

SDSS J130017+263238 ([Fe/H] = −3.65) shows a value of [Si/Fe], [Mg/Fe] and [Ca/Fe], which is higher than the mean value of the sample, but this is not the case for [Ti/Fe].

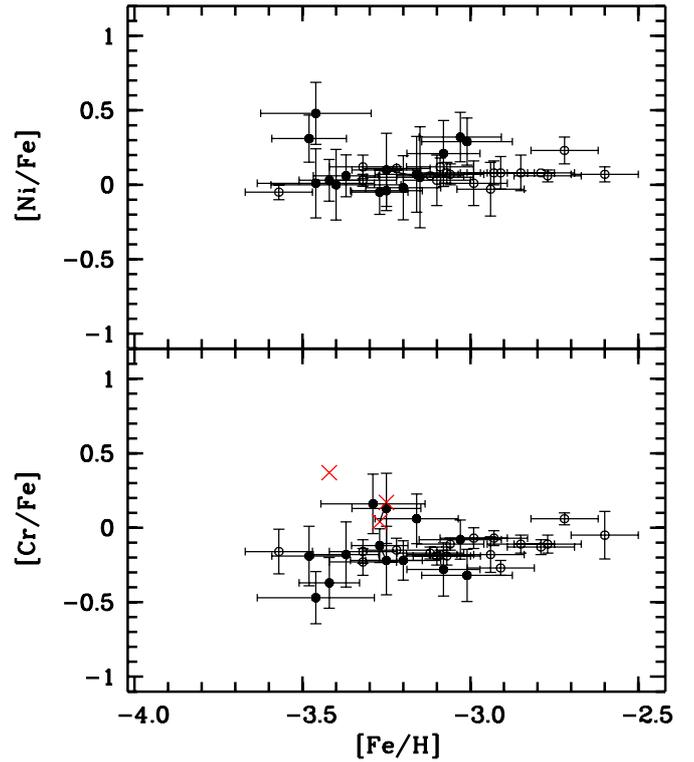The two spectra of SDSS J004029+160416 provide very similar abundances, so that they are not distinguishable in the

Fig. 7. Ratios of even iron-peak elemements to iron for our programme stars (filled circles) compared to those of Bonifacio et al. (2009) (open circles). In the lower panel the two measures of Cr ɪɪ lines are shown as × symbols.

plot. Instead the two spectra of SDSS J002113-005005 imply a difference of 0.1 dex in [Fe/H]; to identify that the two points refer to the same star we connected them with a line in Fig. 6 and all subsequent plots.
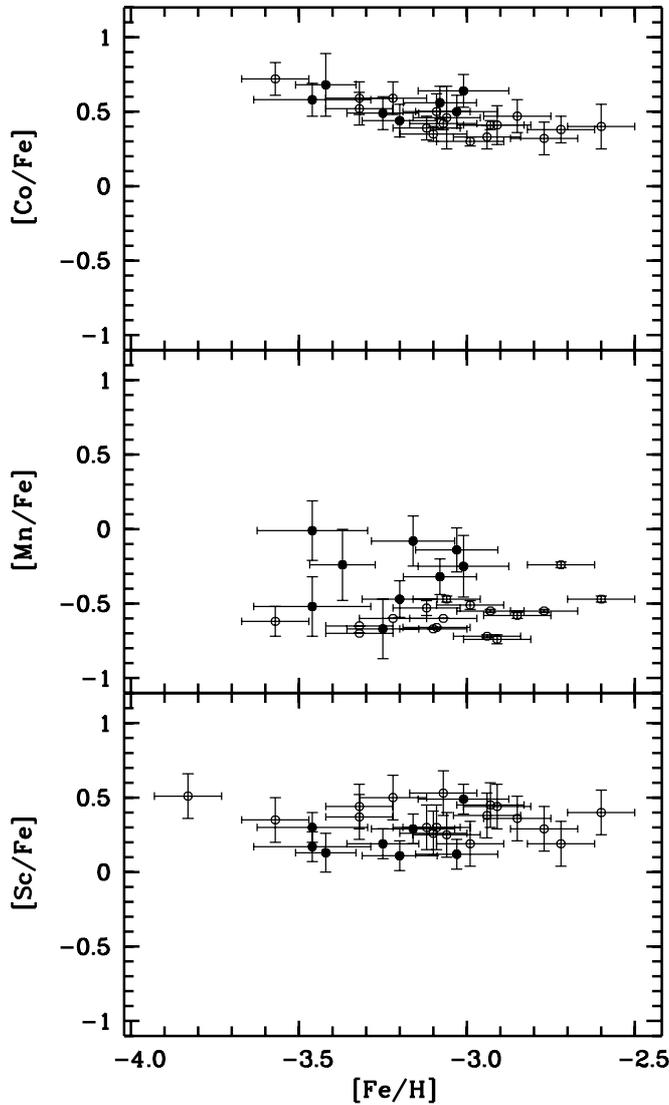
6.2. Even iron peak elements

The abundances of Ni and Cr behave as expected, the decrease of the [Cr/Fe] is probably driven by NLTE effects, as testified by the two measurements of Cr ɪɪ lines and discussed in Bonifacio et al. (2009) and Bergemann & Cescutti (2010). There is one star, SDSS J082521+040334, which has a remarkably high [Ni/Fe] = +0.48, note that this star also has low [Ca/Fe] and [Ti/Fe]. Three more stars have [Ni/Fe] ~ +0.3, SDSS J113528+010848, SDSS J154246+054426 and SDSS J230814−085526. Considering the errors, all these are compatible with [Ni/Fe] ~ 0 at 2σ. The straight mean of all values is ⟨[Ni/Fe]⟩ = 0.13 ± 0.16, again compatible with zero.

6.3. Odd iron peak elements

The elements Sc and Co show a behaviour that totally agrees with that found by Bonifacio et al. (2009). Only Mn is higher on average and a few stars show a [Mn/Fe] that is almost solar, while others show [Mn/Fe] as low as −0.5 dex or lower. Both in the present paper and in Bonifacio et al. (2009) the abundances are derived from the Mn ɪ resonance triplet at 403 nm. In the plots we did not adopt the correction of +0.4 dex suggested by Bonifacio et al. (2009), based on the offset found in giant stars between resonance and high excitiation lines. Bergemann & Gehren (2008) have computed Mn abundances for a sample

Table 8. Galactic coordinates, distances from the Sun and from the Galactic centre, and barycentric radial velocities, for the programme stars.

Star	l	b	Class	d kpc	σ_d kpc	R kpc	v_R km s^{-1}
SDSS J002113−005005	106.2675	−62.7251	MS	3.96	0.07	9.82	−94.2
	106.2675	−62.7251	SG	2.47	0.06	9.15	
SDSS J002749+140418	114.2890	−48.4034	SG	4.30	0.07	10.52	+27.8
SDSS J004029+160416	119.0930	−46.7189	SG	2.32	0.04	9.53	−49.1
	119.0930	−46.7189	SG	2.32	0.04	9.53	
SDSS J031745+002304	180.9504	−45.3647	SG	4.29	0.07	11.91	+113.5
SDSS J082118+181931	205.5011	+27.7892	SG	4.41	0.05	12.31	+162.6
SDSS J082521+040334	220.2941	+22.7044	SG	5.00	0.03	12.53	+10.8
SDSS J090733+024608	227.2893	+31.2990	SG	3.82	0.03	11.16	+313.0
SDSS J113528+010848	264.7169	+58.2657	SG	4.46	0.03	9.79	−88.9
SDSS J122935+262445	220.0458	+85.0737	MS	2.20	0.03	8.92	+66.3
SDSS J130017+263238	16.9469	+87.9415	SG	3.44	0.02	9.06	−77.4
SDSS J143632+091831	2.2179	+59.4609	SG	3.13	0.02	7.42	−113.2
SDSS J144640+124917	10.6982	+59.4938	SG	3.45	0.02	7.41	−110.4
SDSS J154246+054426	13.1225	+44.0248	SG	5.08	0.05	6.13	−123.9
SDSS J223143−094834	53.9497	−52.8171	SG	4.59	0.05	8.10	−5.6
SDSS J230814−085526	64.8229	−59.5785	MS	1.30	0.04	8.32	−111.0
SDSS J233113−010933	83.0480	−57.6812	MS	2.56	0.04	8.72	−101.3

Fig. 8. Ratios of odd iron-peak elements to iron for our programme stars (filled circles) compared to those of the stars of Bonifacio et al. (2009) (open circles).
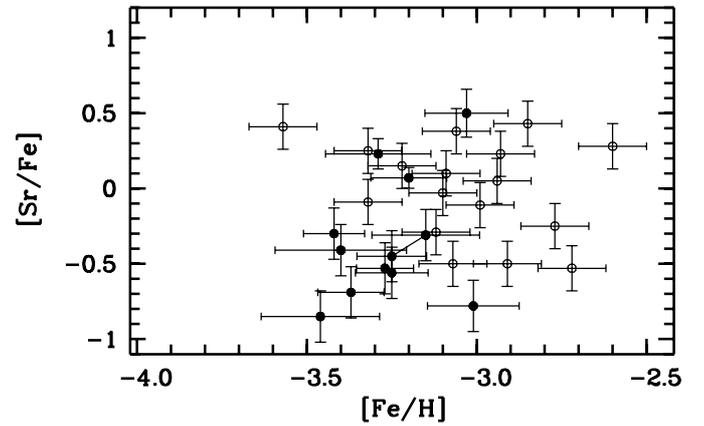
Fig. 9. Ratios of strontium to iron for our programme stars (filled circles) compared to those of the stars of Bonifacio et al. (2009) (open circles).
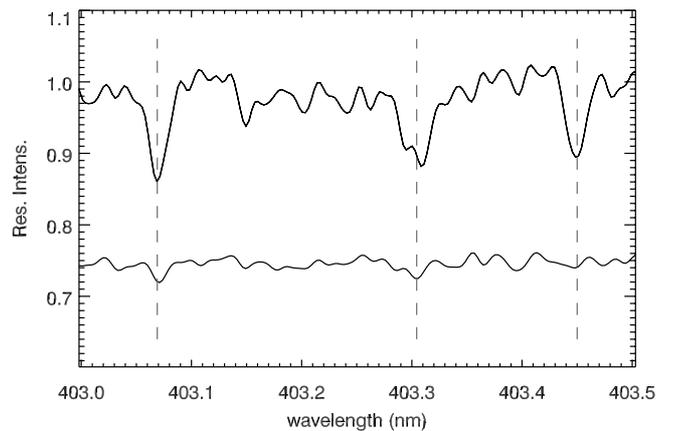
Fig. 10. Mn I 403 nm resonance triplet plotted for star SDSS J144640+124917 (above) and SDSS J004029+160416. The spectra are normalized, and the continuum for star SDSS J004029+160416 was shifted down to 0.75 for readibility. The wavelengths of the three Mn lines are marked. Star SDSS J004029+160416 is 280 K warmer and about 0.1 dex more metal-poor. Gravity is almost the same. [Mn/Fe] = −0.08 in SDSS J144640+124917 and −0.67 in SDSS J004029+160416.
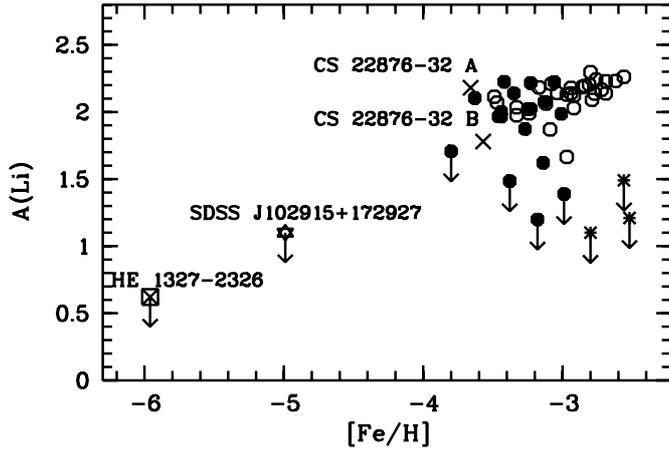
Fig. 11. Lithium abundance as a function of [Fe/H] for our sample of stars (filled hexagons), together with the stars of Sbordone et al. (2010a, open hexagons), the two components of the binary system CS 22876-32 (González Hernández et al. 2008, crosses), the three Li-depleted stars G 122-69, G 139-8, G 186-26 from Norris et al. (1997, asterisks), star SDSS J102915+172927, from Caffau et al. (2011c, star symbol) and star HE 1327-2326 from Frebel et al. (2008, crossed square).
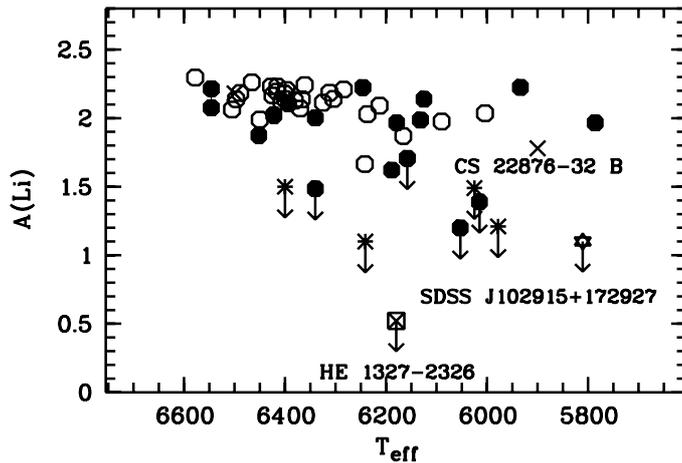

Fig. 12. Lithium abundance as a function of $T_{\rm eff}$, the symbols are the same as in Fig. 11.

of metal-poor dwarfs, and for their model closest to the parameters of our stars ($T_{\rm eff} = 6000$, $\log g = 4.0$, [M/H] = −3.0) they found a sizeable NLTE correction of about 0.6 dex for the resonance triplet, but their computations do not show strong variations of the NLTE corrections with either temperature, metallicity, or gravity. Although a wider set of computations would be desirable, it does seem unlikely that the scatter we observe in Mn abundances is caused by differential NLTE effects. In Fig. 10 we compare two stars whose [Mn/Fe] ratios differ by 0.5 dex, clearly the difference of almost 300 K in effective temperature between the two stars cannot justify the obvious difference in line strength. It is possible that there is some real scatter in Mn abundances, and one should keep in mind that also in the sample of Bonifacio et al. (2009) there are at least two stars with relatively high [Mn/Fe], although at slightly higher metallicities.

6.4. Strontium

Strontium is the only neutron capture element that we are able to measure in this sample of stars. It shows a large scatter in

[Sr/Fe] ratios, as expected (Burris et al. 2000; Barklem et al. 2005; François et al. 2007), and is compatible with the results of Bonifacio et al. (2009).

6.5. Lithium

We measured lithium abundances for 12 stars and provide four upper limits. In Figs. 11 and 12 we show the lithium abundances in our stars. We also added to the plot the stars of Sbordone et al. (2010a) and the two components of the binary system CS 22876-32 (González Hernández et al. 2008, crosses), the three Li-depleted stars G 122-69, G 139-8, G 186-26 from Norris et al. (1997, asterisks), star SDSS J102915+172927 from Caffau et al. (2011c, star symbol) and star HE 1327-2326 from Frebel et al. (2008, crossed square).

Our measured equivalent width of the Li I doublet for star SDSS J090733+024608, agrees excellently with that of Caffau et al. (2011b). This is the only star for which they could measure lithium from the X-Shooter spectra.

The present results reinforce the existence of the meltdown of the Spite plateau at low metallicities, found by Aoki et al. (2009) and Sbordone et al. (2010a). In particular the upper limits, which are quite stringent, call for strong depletions. However, in spite of the evident meltdown it is remarkable that two of the lowest metallicity stars of the sample, SDSS J130017+263238, and SDSS J090733+024608, stay on the Spite plateau, implying that the meltdown is not a mere increase of Li depletion with decreasing metallicity.

It is intriguing that the two most iron-poor objects in the plot, HE 1327-2326 and SDSS J102915+172927, display no lithium. In Figs. 11 and 12 we plot the upper limits as provided by Frebel et al. (2008) and Caffau et al. (2011c), respectively, although in the first case it is a 3σ upper limit, while in the latter it is a 5σ upper limit, by adopting the same criterion the two upper limits would lie roughly at the same level. Caffau et al. (2011c) have pointed out that given the peculiar chemical composition of HE 1327-2326, there is little connection between its iron abundance and its metallicity Z. By plotting the lithium abundances as a function of carbon abundance, rather than of iron abundance, HE 1327-2326 occupies the same region in the diagram as the well-known Li-depleted stars G 122-69, G 139-8 and G 186-26. The known Li-depleted stars are a handful and at [Fe/H] > −3.0 they are only a few percent of the warm halo stars. The fact that in a very limited sample, like ours, we find three new Li-depleted stars suggests that these stars are more frequently found at low [Fe/H]. There is no widely accepted explanation of the Li-depleted stars. Probably the most promising hypothesis is that of Ryan et al. (2002), who measured sizeable rotational velocities in some of the Li-depleted stars and suggested that they are "blue stragglers to be", i.e. although they have colours that are currently compatible with the halo turn-off, in the future, as the TO stars evolve to redder colours, they will remain in their current position in the colour–magnitude diagram. Although it is well known that blue stragglers display no lithium (Glaspey et al. 1994), the reasons for this, or for the blue stragglers phenomenon, for that matter, are not well understood. Although promising, the Ryan et al. (2002) hypothesis does not readily provide any argument that could explain a higher frequency of these objects at low [Fe/H].

There are many mechanisms that can destroy lithium, all of which imply that the material is processed at temperatures exceeding two million degrees. In the present state of affairs it is difficult to argue that one and the same mechanism is responsible

for all the Li-depleted stars. At the same time it is not clear if Li-depleted stars are related to the Spite plateau meltdown.

Figure 12 shows that Li-depleted stars are not confined to a particular range in $T_{\rm eff}$. The hottest Li-depleted star has an effective temperature of 6400 K.

7. Conclusions

Thanks to a very efficient technique of selecting EMP stars from the Sloan Digital Sky Survey, we have considerably increased the sample of stars at the lowest metallicities for which detailed chemical abundances were measured. Note that while in the sample of Bonifacio et al. (2009) there was only one dwarf star with [Fe/H] < −3.4, the present sample comprises six such stars. The agreement between the metallicities estimated from the SDSS spectra and those derived from the UVES spectra suggests that the former are reliable, at least in a statistical sense, for investigating the metallicity distribution of the halo.

The chemical composition of the sample of stars presented here is consistent with that of the sample of Bonifacio et al. (2009), suggesting that the halo was well mixed at all probed metallicities. The only possible exception is a sizeable scatter in Mn abundances. This indication should be taken with caution however, given the lower S/N ratio of the present data compared to that of Bonifacio et al. (2009), and because there are still only few observed stars.

The relatively high S/N ratios in the red part of the spectra allowed us to increase the sample of dwarf stars with measured lithium abundance at metallicities below –3.0. The meltdown of the Spite plateau is confirmed and the three upper limits show the occurance of strong lithium depletions, at least in some cases. On the other hand, the presence at the lowest metallicities of non-depleted stars on the Spite plateau implies that the meltdown depends on some other parameter besides metallicity.

References

Adelman-McCarthy, J. K., Agüeros, M. A., Allam, S. S., et al. 2007, ApJS, 172, 634
Adelman-McCarthy, J. K., Agüeros, M. A., Allam, S. S., et al. 2008, ApJS, 175, 297
Aoki, W., Barklem, P. S., Beers, T. C., et al. 2009, ApJ, 698, 1803
Barklem, P. S., Christlieb, N., Beers, T. C., et al. 2005, A&A, 439, 129
Behara, N. T., Bonifacio, P., Ludwig, H.-G., et al. 2010, A&A, 513, A72
Belokurov, V., Zucker, D. B., Evans, N. W., et al. 2006, ApJ, 642, L137
Bergemann, M., & Cescutti, G. 2010, A&A, 522, A9
Bergemann, M., & Gehren, T. 2008, A&A, 492, 823
Bonifacio, P., & Caffau, E. 2003, A&A, 399, 1183
Bonifacio, P., Pasquini, L., Spite, F., et al. 2002, A&A, 390, 91
Bonifacio, P., Spite, M., Cayrel, R., et al. 2009, A&A, 501, 519
Bonifacio, P., Caffau E., Ludwig, H.-G., et al. 2010, IAU XVII General Assembly, Joint Discussion 5, ed. J. Binney
Bonifacio, P., Caffau, E., François, P., et al. 2011, Astron. Nachr., 332, 251
Bromm, V., & Loeb, A. 2003, Nature, 425, 812
Burris, D. L., Pilachowski, C. A., Armandroff, T. E., et al. 2000, ApJ, 544, 302
Caffau, E., Ludwig, H.-G., Steffen, M., Freytag, B., & Bonifacio, P. 2011a, Sol. Phys., 268, 255
Caffau, E., Bonifacio, P., François, P., et al. 2011b, A&A, 534, A4
Caffau, E., Bonifacio, P., François, P., et al. 2011c, Nature, 477, 67
Caffau, E., Bonifacio, P., François, P., et al. 2012, A&A, 542, A51
Carollo, D., Beers, T. C., Lee, Young, S., et al. 2007, Nature, 450, 1020
Carollo, D., Beers, T. C., Chiba, M., et al. 2010, ApJ, 712, 692
Castelli, F. 2005, Mem. Soc. Astron. Ital. Supp., 8, 25
Cayrel, R. 1988, in The Impact of Very High S/N Spectroscopy on Stellar Physics, ed. G. Cayrel de Strobel, & M. Spite, IAU Symp., 132, 345
Dekker, H., D'Odorico, S., Kaufer, A., Delabre, B., & Kotzlowski, H. 2000, Proc. SPIE, 4008, 534
D'Odorico, S., Dekker, H., Mazzoleni, R., et al. 2006, Proc. SPIE, 6269,
Eggen, O. J., Lynden-Bell, D., & Sandage, A. R. 1962, ApJ, 136, 748
Font, A. S., McCarthy, I. G., Crain, R. A., et al. 2011, MNRAS, 416, 2802
François, P., Depagne, E., Hill, V., et al. 2007, A&A, 476, 935
Frebel, A., Johnson, J. L., & Bromm, V. 2007, MNRAS, 380, L40
Frebel, A., Collet, R., Eriksson, K., Christlieb, N., & Aoki, W. 2008, ApJ, 684, 588
Freytag, B., Steffen, M., & Dorch, B. 2002, Astron. Nachr., 323, 213
Freytag, B., Steffen, M., Ludwig, H.-G., et al. 2012, J. Comp. Phys., 231, 919
Girardi, L., Bertelli, G., Bressan, A., et al. 2002, A&A, 391, 195
Glaspey, J. W., Pritchet, C. J., & Stetson, P. B. 1994, AJ, 108, 271
González Hernández, J. I., Bonifacio, P., Ludwig, H.-G., et al. 2008, A&A, 480, 233
Helmi, A. 2008, A&ARv, 15, 145
Kurucz, R. 1993, SYNTHE Spectrum Synthesis Programs and Line Data, Kurucz CD-ROM No. 18 (Cambridge, Mass.: Smithsonian Astrophysical Observatory)
Kurucz, R. L. 2005, Mem. Soc. Astron. Ital. Supp., 8, 14
Li, H. N., Christlieb, N., Schörck, T., et al. 2010, A&A, 521, A10
Lodders, K., Palme, H., & Gail, H.-P. 2009, in Landolt-Börnstein – Group VI Astronomy and Astrophysics Numerical Data and Functional Relationships in Science and Technology, Vol. 4B, Solar System, ed. J. E. Trümper, 44
Ludwig, H.-G., Bonifacio, P., Caffau, E., et al. 2008, Phys. Scr. T, 133, 014037
Ludwig, H.-G., Caffau, E., Steffen, M., et al. 2009, Mem. Soc. Astron. Italiana, 80, 711
Majewski, S. R. 1992, ApJS, 78, 87
Marigo, P., Girardi, L., Bressan, A., et al. 2008, A&A, 482, 88
Mashonkina, L., Korn, A. J., & Przybilla, N. 2007, A&A, 461, 261
Norris, J. E., Ryan, S. G., Beers, T. C., & Deliyannis, C. P. 1997, ApJ, 485, 370
Piau, L., Beers, T. C., Balsara, D. S., et al. 2006, ApJ, 653, 300
Richards, G. T., Fan, X., Newberg, H. J., et al. 2002, AJ, 123, 2945
Ryan, S. G., & Norris, J. E. 1991, AJ, 101, 1865
Ryan, S. G., Gregory, S. G., Kolb, U., Beers, T. C., & Kajino, T. 2002, ApJ, 571, 501
Salvadori, S., Schneider, R., & Ferrara, A. 2007, MNRAS, 381, 647
Sbordone, L. 2005, Mem. Soc. Astron. Ital. Supp., 8, 61
Sbordone, L., Bonifacio, P., Castelli, F., & Kurucz, R. L. 2004, Mem. Soc. Astron. Ital. Supp., 5, 93
Sbordone, L., Bonifacio, P., Caffau, E., et al. 2010a, A&A, 522, A26
Sbordone, L., Bonifacio, P., Caffau, E., & Ludwig, H.-G. 2010b [arXiv:1009.5210]
Schneider, R., Ferrara, A., Salvaterra, R., Omukai, K., & Bromm, V. 2003, Nature, 422, 869
Schörck, T., Christlieb, N., Cohen, J. G., et al. 2009, A&A, 507, 817
Searle, L., & Zinn, R. 1978, ApJ, 225, 357
Wedemeyer, S., Freytag, B., Steffen, M., Ludwig, H.-G., & Holweger, H. 2004, A&A, 414, 1121
Yanny, B., Rockosi, C., Newberg, H. J., et al. 2009, AJ, 137, 4377
York, D. G., Adelman, J., Anderson, J. E., Jr., et al. 2000, AJ, 120, 1579
Zolotov, A., Willman, B., Brooks, A. M., et al. 2009, ApJ, 702, 1058

Table 1. Log of the observations.

Star	Program	Exposure time	Central wavelength (nm)	Slit width ''	Binning	MJD JD-2 400 000.5	Airmass
		s	nm		days		
SDSS J223143-094834	078.D-0217(A)	3004.999	580	1.4	2 × 2	53995.085976	1.107
SDSS J223143-094834	078.D-0217(A)	3005.001	390	1.4	2 × 2	53995.085987	1.107
SDSS J230814-085526	078.D-0217(A)	3600.001	390	1.4	2 × 2	53997.256895	1.221
SDSS J230814-085526	078.D-0217(A)	3599.999	580	1.4	2 × 2	53997.256899	1.221
SDSS J223143-094834	078.D-0217(A)	3004.999	580	1.4	2 × 2	53998.013442	1.416
SDSS J223143-094834	078.D-0217(A)	3005.001	390	1.4	2 × 2	53998.013452	1.416
SDSS J223143-094834	078.D-0217(A)	3004.999	580	1.4	2 × 2	53998.049319	1.203
SDSS J223143-094834	078.D-0217(A)	3005.001	390	1.4	2 × 2	53998.049330	1.203
SDSS J002113-005005	078.D-0217(A)	3239.999	580	1.4	2 × 2	53998.165339	1.145
SDSS J002113-005005	078.D-0217(A)	3240.001	390	1.4	2 × 2	53998.165349	1.145
SDSS J002113-005005	078.D-0217(A)	3239.999	580	1.4	2 × 2	53998.204093	1.095
SDSS J002113-005005	078.D-0217(A)	3240.001	390	1.4	2 × 2	53998.204116	1.095
SDSS J031745+002304	078.D-0217(A)	3240.001	390	1.4	2 × 2	53998.246345	1.306
SDSS J031745+002304	078.D-0217(A)	3239.999	580	1.4	2 × 2	53998.246361	1.306
SDSS J031745+002304	078.D-0217(A)	3239.999	580	1.4	2 × 2	53998.285346	1.162
SDSS J031745+002304	078.D-0217(A)	3240.001	390	1.4	2 × 2	53998.285356	1.162
SDSS J002749+140418	078.D-0217(A)	3004.999	580	1.4	2 × 2	54002.125063	1.503
SDSS J002749+140418	078.D-0217(A)	3005.001	390	1.4	2 × 2	54002.125073	1.503
SDSS J002749+140418	078.D-0217(A)	3004.999	580	1.4	2 × 2	54002.161983	1.342
SDSS J002749+140418	078.D-0217(A)	3005.001	390	1.4	2 × 2	54002.162032	1.342
SDSS J004029+160416	078.D-0217(A)	3004.999	580	1.4	2 × 2	54003.185786	1.342
SDSS J004029+160416	078.D-0217(A)	3005.001	390	1.4	2 × 2	54003.185797	1.342
SDSS J004029+160416	078.D-0217(A)	3004.999	580	1.4	2 × 2	54003.222459	1.321
SDSS J004029+160416	078.D-0217(A)	3005.001	390	1.4	2 × 2	54003.222535	1.321
SDSS J090733+024608	078.D-0217(A)	3004.999	580	1.4	2 × 2	54085.302979	1.159
SDSS J090733+024608	078.D-0217(A)	3005.001	390	1.4	2 × 2	54085.302990	1.159
SDSS J082521+040334	078.D-0217(A)	3136.999	580	1.4	2 × 2	54086.305133	1.140
SDSS J082521+040334	078.D-0217(A)	3137.001	390	1.4	2 × 2	54086.305159	1.140
SDSS J082521+040334	078.D-0217(A)	3144.999	580	1.4	2 × 2	54100.164555	1.461
SDSS J082521+040334	078.D-0217(A)	3145.001	390	1.4	2 × 2	54100.164618	1.461
SDSS J082521+040334	078.D-0217(A)	3136.999	580	1.4	2 × 2	54100.203967	1.250
SDSS J082521+040334	078.D-0217(A)	3137.001	390	1.4	2 × 2	54100.203982	1.250
SDSS J090733+024608	078.D-0217(A)	3004.999	580	1.4	2 × 2	54100.284761	1.131
SDSS J090733+024608	078.D-0217(A)	3005.001	390	1.4	2 × 2	54100.284775	1.131
SDSS J113528+010848	078.D-0217(A)	3239.999	580	1.4	2 × 2	54132.204936	1.443
SDSS J113528+010848	078.D-0217(A)	3240.001	390	1.4	2 × 2	54132.204950	1.442
SDSS J113528+010848	078.D-0217(A)	3240.000	580	1.4	2 × 2	54132.247986	1.216
SDSS J113528+010848	078.D-0217(A)	3240.001	390	1.4	2 × 2	54132.248000	1.216
SDSS J143632+091831	078.D-0217(A)	3004.999	580	1.4	2 × 2	54133.350058	1.431
SDSS J143632+091831	078.D-0217(A)	3005.001	390	1.4	2 × 2	54133.350074	1.431
SDSS J144640+124917	078.D-0217(A)	3004.999	580	1.4	2 × 2	54158.341745	1.292
SDSS J144640+124917	078.D-0217(A)	3005.001	390	1.4	2 × 2	54158.341760	1.291
SDSS J154246+054426	078.D-0217(A)	3136.999	580	1.4	2 × 2	54174.340722	1.181
SDSS J154246+054426	078.D-0217(A)	3137.001	390	1.4	2 × 2	54174.340741	1.181
SDSS J154246+054426	078.D-0217(A)	3136.999	580	1.4	2 × 2	54177.235829	1.697
SDSS J154246+054426	078.D-0217(A)	3137.001	390	1.4	2 × 2	54177.235847	1.697
SDSS J154246+054426	078.D-0217(A)	3136.999	580	1.4	2 × 2	54177.275076	1.373
SDSS J154246+054426	078.D-0217(A)	3137.001	390	1.4	2 × 2	54177.275094	1.373
SDSS J082118+181931	081.D-0373(A)	3599.997	580	0.6	1 × 1	54583.989490	1.435
SDSS J082118+181931	081.D-0373(A)	3600.001	390	0.6	1 × 1	54583.989571	1.435
SDSS J122935+262445	081.D-0373(A)	3599.997	580	0.8	1 × 1	54584.036879	1.874
SDSS J122935+262445	081.D-0373(A)	3600.001	390	0.8	1 × 1	54584.036926	1.874
SDSS J130017+263238	081.D-0373(A)	3599.997	580	0.8	1 × 1	54584.081867	1.721
SDSS J130017+263238	081.D-0373(A)	3600.001	390	0.8	1 × 1	54584.081909	1.720
SDSS J130017+263238	081.D-0373(A)	3599.997	580	0.8	1 × 1	54584.124756	1.596
SDSS J130017+263238	081.D-0373(A)	3600.001	390	0.8	1 × 1	54584.124810	1.596
SDSS J082118+181931	081.D-0373(A)	3599.997	580	0.8	1 × 1	54585.007509	1.521
SDSS J082118+181931	081.D-0373(A)	3600.001	390	0.8	1 × 1	54585.007553	1.521
SDSS J153110+095255	081.D-0373(B)	3599.997	580	1.0	2 × 2	54700.994156	1.365
SDSS J153110+095255	081.D-0373(B)	3600.001	390	1.0	2 × 2	54700.994233	1.365
SDSS J153110+095255	081.D-0373(B)	4199.997	580	1.0	2 × 2	54701.036850	1.669
SDSS J153110+095255	081.D-0373(B)	4200.001	390	1.0	2 × 2	54701.036954	1.669
SDSS J233113-010933	081.D-0373(B)	3599.997	580	1.0	2 × 2	54701.089799	2.109
SDSS J233113-010933	081.D-0373(B)	3600.001	390	1.0	2 × 2	54701.089846	2.109
SDSS J233113-010933	081.D-0373(B)	3599.997	580	1.0	2 × 2	54701.132475	1.506

Table 1. continued.

Star	Program	Exposure time	Central wavelength	Slit width ″	Binning	MJD JD-2 400 000.5	Airmass
		s	nm			days	
SDSS J233113-010933	081.D-0373(B)	3600.002	390	1.0	2×2	54701.132554	1.506
SDSS J233113-010933	081.D-0373(B)	3599.998	580	1.0	2×2	54701.175114	1.239
SDSS J233113-010933	081.D-0373(B)	3600.002	390	1.0	2×2	54701.175154	1.239
SDSS J002113-005005	081.D-0373(B)	3599.997	580	0.7	1×1	54701.219980	1.203
SDSS J002113-005005	081.D-0373(B)	3600.001	390	0.7	1×1	54701.220019	1.203
SDSS J004029+160416	081.D-0373(B)	3599.997	580	1.0	2×2	54701.264875	1.361
SDSS J004029+160416	081.D-0373(B)	3600.002	390	1.0	2×2	54701.264915	1.361
SDSS J002113-005005	081.D-0373(B)	3599.997	580	0.7	1×1	54701.343975	1.162
SDSS J002113-005005	081.D-0373(B)	3600.001	390	0.7	1×1	54701.344085	1.162
SDSS J002113-005005	081.D-0373(B)	2623.997	580	0.7	1×1	54701.386599	1.337
SDSS J002113-005005	081.D-0373(B)	2620.002	390	0.7	1×1	54701.386639	1.337